Applied Catalysis B: Environmental 300 (2022) 120722

Contents lists available at ScienceDirect

Applied Catalysis B: Environmental

journal homepage: www.elsevier.com/locate/apcatb

High-valent cobalt-oxo species triggers hydroxyl radical for collaborative environmental decontamination

Yang Zong [a], Hua Zhang [a], Xiaomeng Zhang [a], Wen Liu [b], Longqian Xu [a], Deli Wu [a,c,*]

[a] State Key Laboratory of Pollution Control and Resources Reuse, College of Environmental Science & Engineering, Tongji University, Shanghai 200092, China
[b] The Key Laboratory of Water and Sediment Sciences, Ministry of Education, College of Environmental Sciences and Engineering, Peking University, Beijing 100871, China
[c] Shanghai Institute of Pollution Control and Ecological Security, Shanghai 200092, China

ARTICLE INFO

Keywords:
High-valent cobalt-oxo species
Hydroxyl radical
^{18}O-isotope labeling
Substrate and concentration-dependent oxidation

ABSTRACT

The overlooked role of high-valent cobalt-oxo species (Co(IV)) in the Co(II)/peroxymonosulfate (PMS) process was uncovered recently using methyl phenyl sulfoxide (PMSO) as the probe. Herein, we further interestingly found that Co(IV) could trigger hydroxyl radical (•OH) formation, resulting in the oxidized products distribution of PMSO heavily relied on the relative concentration of PMSO. More significantly, the generation of a series of ^{18}O-labeled hydroxylated products (i.e., hydroxylated methyl phenyl sulfone, nitrobenzene and 4-nitrobenzoic acid) in $H_2{}^{18}O$ conclusively verified that •OH was triggered by Co(IV) species. Density functional theory calculation demonstrated that Co(IV) initiated •OH formation via oxo ligand protonation-induced valence tautomerization. Moreover, the oxidative contribution of Co(IV) and •OH on organic degradation was specifically dependent on the type and concentration of the substrate. This study provided deeper insights into the evolution pathway of •OH mediated by Co(IV) species and enriched the understandings on the collaborative oxidation mechanism in Co(IV)-involved processes.

1. Introduction

Cobalt (Co(II))-activated peroxymonosulfate (PMS) process is a highly efficient advanced oxidation process (AOP) for the oxidative abatement of organic contaminants, with the treatment performance is even comparable to the classic Fenton process (i.e., the Fe(II)/H_2O_2 reaction) [1]. Sulfate radical ($SO_4^{\bullet-}$) and hydroxyl radical (•OH) have been widely recognized as the primary reactive species generated via the one electron transfer pathway in the Co(II)/PMS process (Eqs. 1 and 2) [2–4]. However, the overlooked role of high-valent metal-oxo species in various AOPs has drawn intensive attentions recently [5–8]. In our previous work, we also surprisingly found that the Co(II)/PMS process readily oxidize methyl phenyl sulfoxide (PMSO) to the corresponding methyl phenyl sulfone ($PMSO_2$) under acidic conditions, with the η($PMSO_2$) (representing the ratio of Δ$PMSO_2$ to ΔPMSO) of ~100% [9]. Given that the transformation of PMSO to $PMSO_2$ is often indicative of the existence of high-valent metal-oxo speices (Eq. 3) [10–12], we therefore proposed that instead of radical species, high-valent cobalt-oxo species (Co(IV)) is actually the dominant reactive species in the Co(II)/PMS process (Eq. 4) at pH ≤ 6.0 [9]. More importantly, the role of Co(IV) was further strongly suggested using ^{18}O-isotope labeling techniques [9], by taking advantage of the characteristic oxygen atom exchange (OAE) reaction between high-valent metal-oxo species and H_2O (Eq. 5) [13–16], which constitutes one of the most conclusive approach for the detection of such species [17–20].

$$Co(II) + HSO_5^- \rightarrow Co(III) + SO_4^{\bullet-} + OH^- \quad (1)$$

$$SO_4^{\bullet-} + OH^- \rightarrow {}^{\bullet}OH + SO_4^{2-} \quad (2)$$

* Corresponding author at: State Key Laboratory of Pollution Control and Resources Reuse, College of Environmental Science & Engineering, Tongji University, Shanghai 200092, China.
E-mail address: wudeli@tongji.edu.cn (D. Wu).

https://doi.org/10.1016/j.apcatb.2021.120722
Received 2 August 2021; Received in revised form 27 August 2021; Accepted 11 September 2021
Available online 20 September 2021
0926-3373/© 2021 Elsevier B.V. All rights reserved.

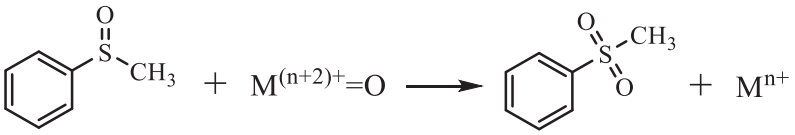

(3)

$$Co(II) + HSO_5^- \rightarrow Co(IV) = O + SO_4^{2-} + H^+ \quad (4)$$

$$Co(IV) = {}^{16}O + H_2{}^{18}O \leftrightarrow Co(IV) = {}^{18}O + H_2{}^{16}O \quad (5)$$

Compared to the widely studied high-valent iron-oxo species (i.e., Fe (IV)/Fe(V)/Fe(VI)) [21–24], the knowledge on Co(IV) species is still rather limited. Recently, the role of Co(IV) in the Co(II)/PMS process was also confirmed in the study by Liu et al. [25]. Similarly, they verified the generation of Co(IV) based on the notable production of $PMSO_2$ and the successful identification of ^{18}O-isotope labeled $PMSO_2$ (noted as $PMS^{16}O^{18}O$) using PMSO as the substrate. Nevertheless, they interestingly found that the newly generated $PMSO_2$ can be further oxidized with the increase in the molar ratio of PMS and Co(II). For instance, under the circumstance that $[PMS]_0$: $[Co(II)]_0$ was 5:1, $PMSO_2$ was slightly degraded after reaching the peak value. And the formed $PMSO_2$ was even completely consumed when $[PMS]_0$: $[Co(II)]_0$ increased to 100:1. Therefore, Liu et al. proposed that the dominant species shifted from Co(IV) to $SO_4^{\bullet-}$ with the increase of $[PMS]_0$: $[Co(II)]_0$. This study is of great significance and provides new understandings regarding the Co (II)/PMS process. However, it is still questionable that if $SO_4^{\bullet-}$ was the main reactive species accounting for the degradation of $PMSO_2$ and why $PMSO_2$ was still remarkably generated in the initial stage of the reaction at $[PMS]_0$: $[Co(II)]_0 = 100:1$, if the dominant species had shifted from Co(IV) to $SO_4^{\bullet-}$ at high $[PMS]_0/[Co(II)]_0$ values, which needs further detailed investigations. Besides, it is also important to elucidate why such phenomena were not observed in our previous study if radical species indeed notably contributed to organics oxidation in this process, and by which pathway is the radical generated (directly induced by the Co(II)/PMS reaction or possibly related to Co(IV)), considering that the obtained results might broaden the knowledge on the Co(II)/PMS process and high-valence metal chemistry.

Encouragingly, the role of Co(IV) species has recently been extended to other Co(II)/peroxide process (e.g., the Co(II)/peracetic acid (PAA) process) [26], in which acetylperoxyl radical and acetoxyl radical are previously considered as the main working oxidants under neutral conditions [27,28]. It was found that similar to the Co(II)/PMS process, the Co(II)/PAA process can also remarkably convert PMSO to $PMSO_2$ under acidic conditions, with $\eta(PMSO_2)$ close to 100%. And the generation of Co(IV) was further proved by ^{18}O-isotope labeling experiments and in-situ Raman spectroscopic characterizations [26]. Nevertheless, despite of these research progresses on the overlooked role of Co(IV) in different AOPs, there are still debates regarding the formation of Co(IV) species. For instance, Li et al. proposed that Co(IV) was unlikely to be generated in the Co(II)/PMS process but believed that the Co(II)−PMS complex was the predominant reactive oxidant [29]. However, this hypothesis seemed cannot rationalize some critical experimental observations in the Co(II)/PMS process as would be discussed below.

Accordingly, based on the above-mentioned advances and controversy, the main purposes of this study are to (1) further clarify the role of radical species ($SO_4^{\bullet-}$ and/or $^{\bullet}OH$) in the Co(II)/PMS process; (2) experimentally and theoretically elucidate the evolution pathway of radical species; (3) evaluate the respective contribution of Co(IV) and $SO_4^{\bullet-}$ or $^{\bullet}OH$ on the oxidative abatement of various representative contaminants, if radical species indeed played a non-negligible role in the studied process.

2. Experimental section

2.1. Chemicals and reagents

Cobalt sulfate heptahydrate ($CoSO_4.7H_2O$, 99.99%) and PMS ($KHSO_5{\cdot}0.5KHSO_4{\cdot}0.5K_2SO_4$, 42–46% $KHSO_5$ basis) were purchased from Macklin Biochemical Technology Co., Ltd. (Shanghai, China). PMSO (>98.0%) and $PMSO_2$ (>97.0%) were supplied by Aladdin Biological Technology Co., Ltd. $H_2{}^{18}O$ (97% ^{18}O-enrichment) was received from Shanghai Engineering Research Center of Stable Isotope. Other chemicals and reagents are listed in Text S1 in Supporting Information (SI).

2.2. Experimental procedure

Except ^{18}O-isotope labeling experiments were conducted in 2.0 mL of $H_2{}^{18}O$, all other batch experiments were performed in 250 mL quartz beakers containing 200 mL of reaction solution (including Co(II), PMS, PMSO or organic contaminant, etc.) with magnetic stirrers under room temperature (22 ± 2 ℃). In a typical procedure, 0.4 mL of Co(II) (0.1 M) and 0.4 mL of PMS (0.1 M) stock solution were successively dosed into 199.2 mL of ultrapure water containing organic contaminant or other chemicals (e.g, PMSO) to initiate the reaction, with pH adjusted to the presetting value using sodium hydroxide or nitric acid in advance. For batch experiments conducted at pH ≤ 3.0, no buffers were employed since the pH value remained stable throughout the reaction. For experiments performed under higher pH conditions (4.0 −6.0), either 10 mM of acetic buffer or an automatic pH titration system (Metrohm 905 Titrando, Switzerland) was used to keep a stable pH value. Note that phosphate buffer was not chosen since the complexation between Co(II) and phosphate might alter the mechanism of the Co (II)/PMS reaction. The total addition of NaOH solution (~0.05 M) during the reaction by the automatic pH titration system was no more than 1.0 mL (200 mL of reaction solution), which exerted a negligible influence on the concentration of the reactants and products. At predetermined time intervals, 1.5 mL of the reacting solution was withdrawn and filtered through polyethersulfone membrane (0.22 μm), with 900 μL of the filtered solution immediately mixed with 100 μL of dimethyl sulfoxide (DMSO) to scavenge the residual PMS and any other transient species, then for further analysis. For samples requiring LC-MS/MS measurements, solid phase extraction columns (Poly-Sery HLB cartridge (200 mg) (ANPEL, Shanghai)) were used to extract and desalinate the reaction products.

2.3. Analytical methods

The pH values were monitored by a HACH HQ11d pH meter. The concentration of organics was quantified by Agilent 1260 high performance liquid chromatography equipped with a diode array detector, and the organic compounds were separated by a ZORBAX Eclipse XDB-C18 column (4.6 × 150 mm, 5 μm; Agilent Co.), with detection details

are presented in Text S2 and Table S1. Ultrahigh performance liquid chromatography-quadrupole time-of-flight mass spectrometer (UPLC-Q-TOF MS/MS) was used to qualitatively and semi-quantitatively determine $PMSO_2$, $PMSO_2$-related chemicals and degradation products of contaminants. $PMS^{16}O^{16}O$ (theoretical $m/z = 157.0318$ $[M + H]^+$) and $PMS^{16}O^{18}O$ (theoretical $m/z = 159.0360$ $[M + H]^+$) were determined in positive electrospray ionization (ESI+) mode. Hydroxylated $PMSO_2$ (noted as $PMS^{16}O^{16}O{-}{}^{16}OH$, theoretical $m/z = 171.0110$ $[M - H]^-$), ^{18}O isotope-labeled hydroxylated $PMSO_2$ (noted as $PMS^{16}O^{18}O{-}{}^{16}OH/PMS^{16}O^{16}O{-}{}^{18}OH$, theoretical $m/z = 173.0152$ $[M - H]^-$; $PMS^{16}O^{18}O{-}{}^{18}OH$, theoretical $m/z = 175.0194$ $[M - H]^-$) and all other hydroxylated products were determined in negative electrospray ionization (ESI−) mode to obtain higher signal/noise ratio and better data quality. The theoretical m/z of the target compounds in ESI+ or ESI− mode were determined using Compass IsotopePattern software (Bruker, Germany). Extracted ion chromatogram (EIC) was employed for the targeted screening of the desired compounds based on the corresponding theoretical m/z. To ensure the measured m/z values are as precise as possible, sodium formate (100 ppm) was simultaneously injected into the mass spectrometer during the analysis, for MS calibration, with the flow rate of 0.09 mL/h. For instance, the first peak with the retention time of 0.14 min in Fig. S1a represents sodium formate. More details in UPLC-Q-TOF MS/MS measurements are recorded in Text S2.

2.4. Density functional theory (DFT) calculations

The Gaussian 09 program was employed for DFT calculations [30]. Geometry optimization was performed at PBE0-D3BJ/TZVP level [31,32], followed by frequency calculation to obtain Gibbs free energy at room temperature at the same level. Both the stability of wavefunction and spin multiplicity was examined for each compound and the ground state was presented. The solvent effect of water was taken into account by a solvation model based on density (SMD). Two explicit water molecules was introduced to correctly describe the solvation of proton.

3. Results and discussion

3.1. $^{\bullet}OH$ is generated in the Co(II)/PMS process but it depends

The degradation of PMSO and the generation of $PMSO_2$ (represented as ΔPMSO and $\Delta PMSO_2$, respectively) were investigated in the Co(II)/PMS process using PMSO as the substrate at $[PMS]_0$: $[Co(II)]_0 = 1{:}1$. As indicated in Fig. 1, PMSO was readily oxidized to $PMSO_2$, with $\eta(PMSO_2)$ of ~100% when $[PMSO]_0$ (500 or 250 μM) was excessive than $[PMS]_0$ (200 μM). And the maximum ΔPMSO and $\Delta PMSO_2$ could reached to 172.6 μM and 171.8 μM, respectively, which are close to the theoretical maximum ΔPMSO and $\Delta PMSO_2$ (200 μM), thereby suggesting the dominant role of Co(IV) species and the remarkable oxidizing capacity of the Co(II)/PMS process. These results were consistent with our previous work that $PMSO_2$ could be massively generated in the Co(II)/PMS process at pH = 3.0 [9]. However, Fig. 1 also showed that the newly formed $PMSO_2$ was further degraded when $[PMSO]_0$ (50 or 10 μM) was much lower than $[PMS]_0$ (200 μM). For instance, at $[PMSO]_0 = 10$ μM, the generated $PMSO_2$ was rapidly consumed after reaching to the peak value of 9.7 μM (Fig. 1b), with $\eta(PMSO_2)$ was merely 8.2% after reacting for 60 min, then followed by a slowly decrease to 6.9% in 180 min (Fig. 1c). Therefore, it can be concluded that $[PMSO]_0$ significantly affected $\eta(PMSO_2)$ and probably influenced the oxidized products distribution of PMSO in the Co(II)/PMS process. Interestingly, as illustrated in Fig. S1 and S2, UPLC-Q-TOF MS/MS analysis indicated that the further degradation products of $PMSO_2$ in the Co(II)/PMS process were mainly hydroxylated $PMSO_2$ (noted as $PMSO_2{-}OH$, theoretical $m/z = 171.0110$ $[M - H]^-$), consistent with the oxidized products of $PMSO_2$ in the Fe(II)/H_2O_2 process in which $^{\bullet}OH$ is generated as the dominant species (Fig. S3). These results implied that the consumption of $PMSO_2$ in the Co(II)/PMS process might be associated with $^{\bullet}OH$.

Nevertheless, $PMSO_2{-}OH$ was also unexpectedly detected during the oxidation of $PMSO_2$ in the UV/PDS process (i.e., authentic source of $SO_4^{\bullet-}$), even in the presence of 25 mM of TBA to scavenge the possibly generated $^{\bullet}OH$ (Fig. S4). However, it was noteworthy that different from the Co(II)/PMS process, $PMSO_2{-}OH$ were not the most abundant degraded products in the UV/PDS/TBA process. This was ascribed to that although electron transfer and hydrogen abstraction are the main reaction mechanisms between $SO_4^{\bullet-}$ and organic compounds [33,34], hydroxylated or direct $SO_4^{\bullet-}$ addition products could be still generated, which is recognized as a minor pathway [35]. Besides, except for $^{\bullet}OH$ and $SO_4^{\bullet-}$, high-valent metal-oxo species can also result in the formation of hydroxylated products via the oxygen-rebound mechanism [36,37]. Therefore, to further identify the reactive species responsible for the formation of $PMSO_2{-}OH$ in the Co(II)/PMS process, *tert*-butyl alcohol (TBA) was employed to distinguish the respective role of Co(IV), $SO_4^{\bullet-}$ and $^{\bullet}OH$, given that TBA is almost unreactive to high-valent metal-oxo species (e.g., Fe(IV), Co(IV), etc.) but readily scavenge $^{\bullet}OH$ ($k_{^{\bullet}OH + TBA} = (3.8 - 7.6) \times 10^8$ M^{-1} s^{-1}) [9,38,39], and the above result also indicated that TBA cannot, at least remarkably, terminate the reaction between $PMSO_2$ and $SO_4^{\bullet-}$. Fig. S5 showed that 10 mM of TBA exerted no inhibitory effect on the formation of $PMSO_2$, but completely prevented the generated $PMSO_2$ from being further degraded, thus verifying that $^{\bullet}OH$ indeed played a dominant role in the consumption of $PMSO_2$, instead of $SO_4^{\bullet-}$ or Co(IV) species.

Similar results were also observed under other $[PMS]_0/[Co(II)]_0$ molar ratios. As indicated in Fig. S6, at $[PMS]_0$: $[Co(II)]_0 = 10{:}1$ or 1:10, the produced $PMSO_2$ was further degraded when $[PMSO]_0$ was only 10 or 50 μM. TBA scavenging experiments also indicated that $^{\bullet}OH$ was

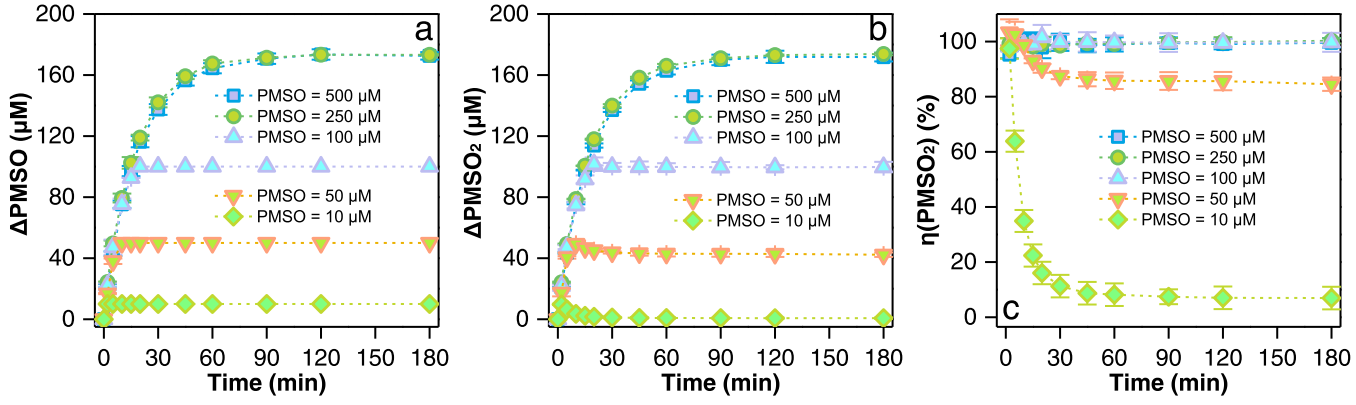

Fig. 1. ΔPMSO (a), $\Delta PMSO_2$ (b) and $\eta(PMSO_2)$ (c) during the oxidation of PMSO in the Co(II)/PMS process under different initial PMSO concentration. Reaction conditions: pH = 3.0, $[Co(II)]_0 = 0.2$ mM, $[PMS]_0 = 0.2$ mM, $[PMSO]_0 = 10 - 500$ μM.

responsible for the degradation of $PMSO_2$ under these tested conditions (Fig. S7). Nonetheless, it was notable that the formed $PMSO_2$ was only moderately oxidized at $[PMS]_0$: $[Co(II)]_0 = 1{:}10$ (Fig. S6), which might be attributed to the scavenging effect of excessive Co(II) towards $^{\bullet}OH$ (Eq. 6). This hypothesis was further verified by the deteriorated decay ratio of $PMSO_2$ in the Co(II)/PMS process with the increase of Co(II) dosage (Fig. S8a). Besides, as shown in Fig. S8b, the generation of $^{\bullet}OH$ was also verified by the successful detection of *p*-hydroxybenzoic acid using benzoic acid as trapping agent for $^{\bullet}OH$ [40,41]. However, despite that the contribution of $^{\bullet}OH$ was proved under all the tested $[PMS]_0/[Co(II)]_0$ molar ratios, it seemed that the oxidative role of $^{\bullet}OH$ can be only notably revealed under insufficient $[PMSO]_0$ (Fig. 1 and S6). UPLC-Q-TOF MS/MS analysis further supported that the formation of $PMSO_2$−OH was indeed significantly suppressed at $[PMSO]_0 = 500$ μM compared to that at $[PMSO]_0 = 50$ μM (Fig. S9). These abnormal results interestingly implied that $^{\bullet}OH$ might not be directly generated by the Co(II)/PMS reaction, but was somehow originated from Co(IV) species.

$$Co(II) + {}^{\bullet}OH \rightarrow Co(III) + OH^- \quad (6)$$

3.2. Co(IV)-triggered generation of $^{\bullet}OH$ evidenced by ^{18}O-isotope labeling techniques

To verify if the evolution of $^{\bullet}OH$ in the Co(II)/PMS process was possibly associated with Co(IV) species, ^{18}O-isotope labeling experiments were conducted. As illustrated in Fig. 2a, b and S10, in the $H_2{}^{18}O$ matrix, $PMS^{16}O^{16}O$ ($m/z = 157.0318 \pm 0.002$ $[M + H]^+$) and $PMS^{16}O^{18}O$ ($m/z = 159.0360 \pm 0.002$ $[M + H]^+$) were successfully identified in the Co(II)/PMS process, by comparing with the authentic sample of $PMS^{16}O^{16}O$ (Fig. S11), which verified the formation of Co(IV) species. However, the ratios of $PMS^{16}O^{18}O$ to $PMSO_2$ (the sum of $PMS^{16}O^{16}O$ and $PMS^{16}O^{18}O$) at $[PMS]_0$: $[Co(II)]_0 = 10{:}1$ (Fig. 2a) and 1:10 (Fig. 2b) were notably different, which were determined to be 11.9% and 61.3%, respectively. Such a discrepancy was attributed to the interference of the direct oxidation of PMSO to $PMSO_2$ by PMS alone via an oxygen atom transfer step (Eq. 7) [9]. Under excessive PMS dosage, PMS inevitably consumed a portion of PMSO despite of the relatively slow reaction rate constant ($k_{PMS + PMSO} = 0.10\ M^{-1}\ s^{-1}$) [9]. However, PMS cannot undergo OAE reaction with H_2O and thereby absolute no $PMS^{16}O^{18}O$ was generated from the reaction between PMS and PMSO in $H_2{}^{18}O$ (Fig. S12), consequently lowering the ratio of $PMS^{16}O^{18}O$ to $PMSO_2$ at $[PMS]_0$: $[Co(II)]_0 = 10{:}1$. While at $[PMS]_0$: $[Co(II)]_0 = 1{:}10$, the direct reaction between PMS and PMSO was strongly suppressed due to the excessive dosage of Co(II), thus in our previous work and the work by Liu et al., the ratio of $PMS^{16}O^{18}O$ to $PMSO_2$ was ~50% at $[PMS]_0$:$[Co(II)]_0 = 1{:}1$ [9,25], which was between those at $[PMS]_0$:$[Co(II)]_0 = 10{:}1$ and 1:10 in this work.

$$HSO_5^- + PMSO \rightarrow SO_4^{2-} + PMSO_2 + H^+ \quad (7)$$

More interestingly, at $[PMS]_0$:$[Co(II)]_0 = 10{:}1$, we further successfully detected the generation of $PMS^{16}O^{16}O{-}{}^{16}OH$ ($m/z = 171.0110 \pm 0.002$ $[M - H]^-$), $PMS^{16}O^{16}O{-}{}^{18}OH/PMS^{16}O^{18}O{-}{}^{16}OH$ ($m/z = 173.0152 \pm 0.002$ $[M - H]^-$) and $PMS^{16}O^{18}O{-}{}^{18}OH$ ($m/z = 175.0194 \pm 0.002$ $[M - H]^-$) using $PMS^{16}O$ as the substrate in $H_2{}^{18}O$ (Fig. 2c and S13), which supported the formation of ^{18}O-isotope labeled $^{\bullet}OH$ (noted as $^{\bullet}{}^{18}OH$) in the Co(II)/PMS process. However, as comparison, only $PMS^{16}O^{16}O{-}{}^{16}OH$ but no ^{18}O-incorporated products were generated during the oxidation of $PMS^{16}O^{16}O$ in the Fe(II)/H_2O_2 process in $H_2{}^{18}O$ (Fig. S14), suggesting that same to PMS, $^{\bullet}OH$ and $PMS^{16}O^{16}O{-}{}^{16}OH$ cannot undergo OAE reaction themselves with H_2O and thereby neither $^{\bullet}{}^{18}OH$ nor $PMS^{16}O^{16}O{-}{}^{18}OH$ would be produced in high-valent metal-oxo species-absent processes. To further verify the formation of ^{18}O-incorporated hydroxylated products in the Co(II)/PMS process, the oxidation of $PMS^{16}O^{16}O$ in $H_2{}^{18}O$ was directly investigated. Fig. S15 illustrated that $PMS^{16}O^{16}O{-}{}^{18}OH$ was indeed generated, with the ratio of $PMS^{16}O^{16}O{-}{}^{18}OH$ to $PMSO_2$−OH (the sum of $PMS^{16}O^{16}O{-}{}^{18}OH$ and $PMS^{16}O^{16}O{-}{}^{16}OH$) determined to be 51.3%. This value was

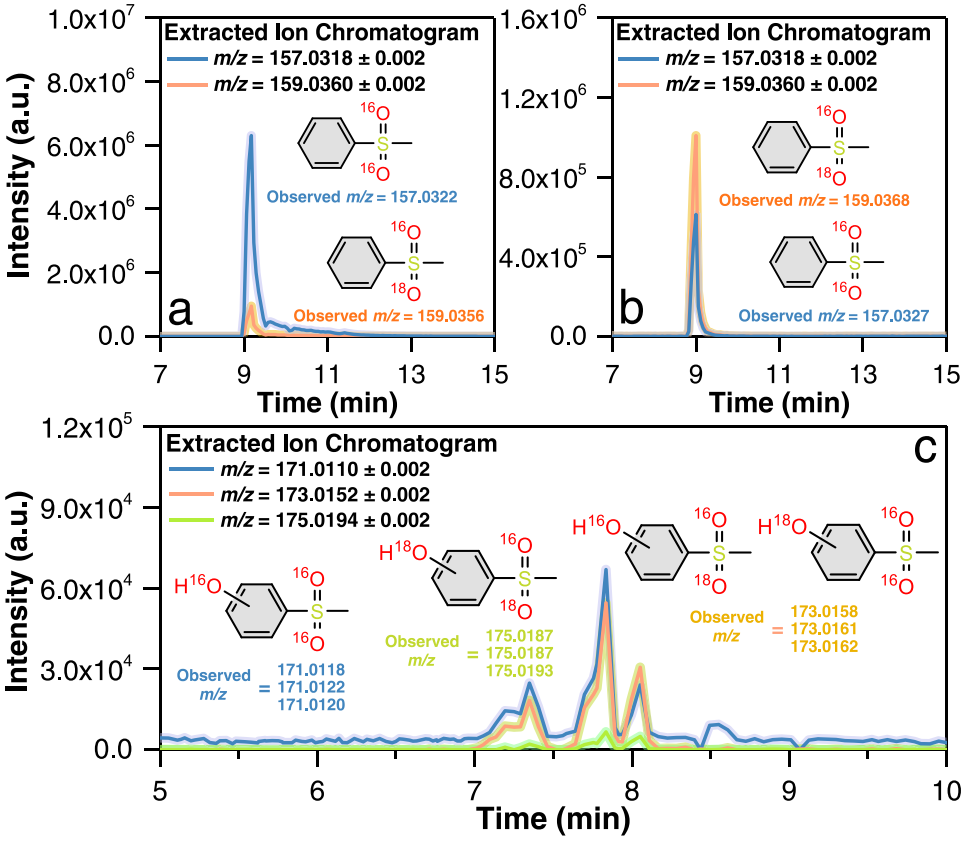

Fig. 2. EIC of $PMS^{16}O^{16}O$ ($m/z = 157.0318 \pm 0.002$ $[M + H]^+$) and $PMS^{16}O^{18}O$ ($m/z = 159.0360 \pm 0.002$ $[M + H]^+$) generated during the oxidation of $PMS^{16}O$ in the Co(II)/PMS process in $H_2{}^{18}O$ at $[PMS]_0$: $[Co(II)]_0 = 10{:}1$ (a) and 1:10 (b), EIC of $PMS^{16}O^{16}O{-}{}^{16}OH$ ($m/z = 171.0110 \pm 0.002$ $[M - H]^-$), $PMS^{16}O^{16}O{-}{}^{18}OH/PMS^{16}O^{18}O{-}{}^{16}OH$ ($m/z = 173.0152 \pm 0.002$ $[M - H]^-$) and $PMS^{16}O^{18}O{-}{}^{18}OH$ ($m/z = 175.0194 \pm 0.002$ $[M - H]^-$) generated during the oxidation of $PMS^{16}O$ in the Co(II)/PMS process in $H_2{}^{18}O$ at $[PMS]_0$:$[Co(II)]_0 = 10{:}1$ (c). Reaction conditions: pH = 3.0, $[Co(II)]_0 = 0.2$ mM for (a, c) and 20 mM for (b), $[PMS]_0 = 2.0$ mM, $[PMS^{16}O]_0 = 0.5$ mM. The experimental data in Figs. 2a and 2c were collected from the same sample.

close to that of $PMS^{16}O^{18}O$ to $PMSO_2$ (61.3%) at $[PMS]_0$:$[Co(II)]_0$ = 1:10 in Fig. 2b, under which conditions the ratio of $PMS^{16}O^{18}O$ to $PMSO_2$ was more representative of the OAE reaction rate between Co (IV) and H_2O since the direct reaction between PMS and PMSO was restrained. Hence, such a consistency demonstrated that the evolution of •OH was strongly associated with Co(IV) species. Moreover, the ratio of $PMS^{16}O^{16}O-^{18}OH$ to $PMSO_2-OH$ (51.3%) obtained in the oxidation of $PMS^{16}O^{16}O$ could also reasonably explain why that of $PMS^{16}O^{16}O-^{16}OH$:$PMS^{16}O^{16}O-^{18}OH$/$PMS^{16}O^{18}O-^{16}OH$:$PMS^{16}O^{18}O-^{18}OH$ in Fig. 2c was ascertained to be 47.4%: 47.0%: 5.6% (see detailed analysis in Fig. S16). In addition, under the $[PMS]_0/[Co(II)]_0$ ratio of 1: 10, the generation of $PMS^{16}O^{16}O-^{16}OH$, $PMS^{16}O^{16}O-^{18}OH$/$PMS^{16}O^{18}O-^{16}OH$ and $PMS^{16}O^{18}O-^{18}OH$ was also confirmed (Fig. S17), despite that the corresponding intensities were much lower than those at $[PMS]_0$: $[Co(II)]_0$ = 10: 1, due to the scavenging effect of excessive Co (II) on •OH as mentioned above.

3.3. Deteriorated conversion of Co(IV) to •OH with the increase of pH

The degradation of PMSO and the formation of $PMSO_2$ beyond pH = 3.0 were also investigated. However, under acetic-buffered conditions (pH = 4.0 and 5.0), we only detected the notable generation of $PMSO_2$, yet the newly formed $PMSO_2$ was not further consumed, even under relatively low $[PMSO]_0$ (Fig. S18), which was quite different from the observations at pH = 3.0 as discussed above. We concluded it was partially because of the scavenging reaction of acetic buffer towards •OH ($k_{acetic\ acid + {}^{\bullet}OH} = (1.6 - 8.5) \times 10^7\ M^{-1}\ s^{-1}$) [42], which was evidenced by that the addition of acetic acid at pH = 3.0 notably suppressed the further degradation of $PMSO_2$ (Fig. S19). These results also elucidated why the formed $PMSO_2$ was not degraded and the role of •OH was unremarkable in the Co(II)/PAA process [26], despite that Co(IV) was found as a predominant reactive species under acidic conditions in this process.

^{18}O-isotope labeling experiments using $PMS^{16}O$ as the substrate were conducted at pH = 4.0, 5.0 and 6.0 in the Co(II)/PMS process as well. As expected, Fig. 3a showed that $PMS^{16}O^{18}O$ were notably detected, which further suggested the generation of Co(IV) species in the pH range of 4.0 − 6.0. The formation of $PMS^{16}O^{16}O-^{18}OH$ and $PMS^{16}O^{18}O-^{18}OH$ was also confirmed at pH = 4.0 (Fig. 3b), indicating that Co(IV) similarly triggered •OH under this pH value. However, it was noteworthy that the abundance of ^{18}O-incorporated $PMSO_2-OH$ generated at pH = 4.0 was much lower than that at pH = 3.0 under identical conditions, and $PMS^{16}O^{16}O-^{18}OH$ was barely detected at pH = 5.0 and 6.0 (Fig. S20). Except for the scavenging reaction between acetic acid and •OH under buffered conditions, deteriorated conversion of Co(IV) to •OH might also account for the decreased formation of ^{18}O-labeled $PMSO_2-OH$. Therefore, to exclude the interference of acetic acid or any other buffer species, the degradation of PMSO and the generation of $PMSO_2$ were again investigated at pH = 4.0 using an automatic pH titration system to keep a stable pH throughout the reaction. Fig. S21 indicated that a relatively low $[PMSO]_0$ was likewise beneficial to the further consumption of the generated $PMSO_2$, but the extent of $PMSO_2$ degradation indeed narrowed compared to that at pH = 3.0. Combined with the results obtained under a more acidic condition (pH = 2.6, Fig. S22), it can be concluded that the reaction rate between Co(II) and PMS increased with pH, but the transformation pathway of Co(IV) to •OH deteriorated with pH variation from acidic conditions to near-neutral conditions.

3.4. DFT calculation on the evolution pathway of •OH initiated by Co(IV) species

It was reported that Fe(IV) can react with H_2O to generate •OH (Eq. 8, $k = 1.3 \times 10^{-2}\ s^{-1}$) [43–45]. As the counterpart of Fe(IV), Co(IV) is expected to be a more reactive species than Fe(IV) according to the oxo-wall rule [16,46,47], thus the formation of •OH in the Co(II)/PMS process was possibly originated from the reaction between Co(IV) and H_2O. However, this assumption implied that ^{18}O-labeled hydroxylated products should account for 100% of the total hydroxylated products in $H_2{}^{18}O$, which was contradictory to the above results, for instance, in Fig. 2c and S15. Alternatively, it was also documented that in Fe(II) and Fe(IV)-involved process, •OH could be generated via the self-decay of Fe (IV) to form H_2O_2 and the subsequent Fenton reaction [48]. Nonetheless, this reaction scheme was unlikely the source of •OH in the Co (II)/PMS process, in consideration that there is still no literature proving the conversion of Co(IV) to H_2O_2, and Co(II) itself is also extremely ineffective in activating H_2O_2 to produce •OH [2,49].

$$Fe(IV) = O + H_2O \rightarrow {}^{\bullet}OH + Fe(III) + OH^- \quad (8)$$

To have deeper mechanistic insights into the evolution pathway of •OH triggered by Co(IV) species, DFT calculation was conducted, with the optimized model sketches and detailed information of intermediate (INT) and transition states (TS) were recorded in Fig. S23 and Tables S2–S7. The spin multiplicity of Co(IV) species ($Co^{IV}(H_2O)_5O^{2+}$) was ascertained to be 4 due to a lower relative free energy compared to that of 2 (Fig. 4). In the proposed calculation model for the conversion of Co(IV) to •OH, $Co^{IV}(H_2O)_5O^{2+}$ first underwent the protonation of oxo ligand via TS_1 with an energy barrier of 12.7 kcal mol^{-1}, resulting in the formation of INT_1 ($Co^{IV}(H_2O)_5OH^{3+}$, Eq. 9). Afterwards, $Co^{IV}(H_2O)_5OH^{3+}$ released •OH via the valence tautomerization (TS_2)

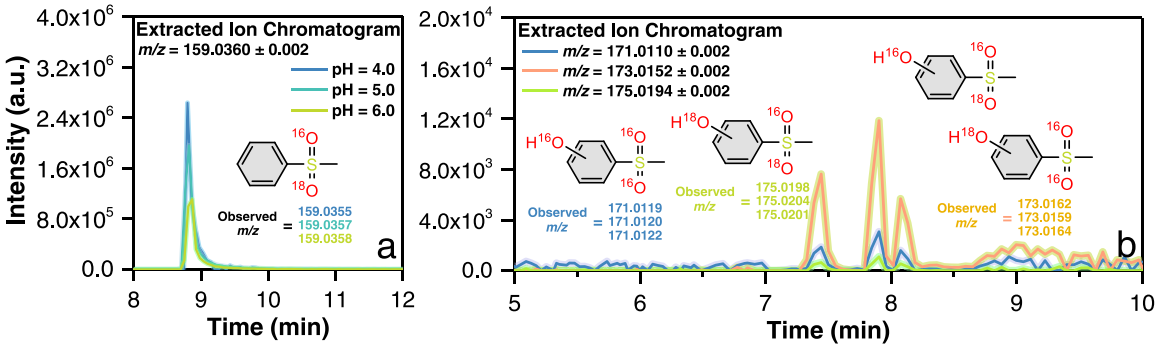

Fig. 3. EIC of $PMS^{16}O^{18}O$ (m/z = 159.0360 ± 0.002 $[M + H]^+$) generated during the oxidation of $PMS^{16}O$ in the Co(II)/PMS process in $H_2{}^{18}O$ at pH = 4.0, 5.0 and 6.0 (a), EIC of $PMS^{16}O^{16}O-^{16}OH$ (m/z = 171.0110 ± 0.002 $[M - H]^-$), $PMS^{16}O^{16}O-^{18}OH$/$PMS^{16}O^{18}O-^{16}OH$ (m/z = 173.0152 ± 0.002 $[M - H]^-$) and $PMS^{16}O^{18}O-^{18}OH$ (m/z = 175.0194 ± 0.002 $[M - H]^-$) generated during the oxidation of $PMS^{16}O$ in the Co(II)/PMS process in $H_2{}^{18}O$ at pH = 4.0 (b). Reaction conditions: $[Co(II)]_0$ = 2.0 mM for (a) and 0.2 mM for (b), $[PMS]_0$ = 2.0 mM, $[PMS^{16}O]_0$ = 0.5 mM, acetic buffer = 100 mM for (a) and 25 mM for (b). Note that the concentration of acetic buffer for (b) was lower than that for (a), to minimize the scavenging reaction between acetic acid and •OH, without notably compromising the buffering capacity. The pH variation during the reaction was less than 0.25 for (b).

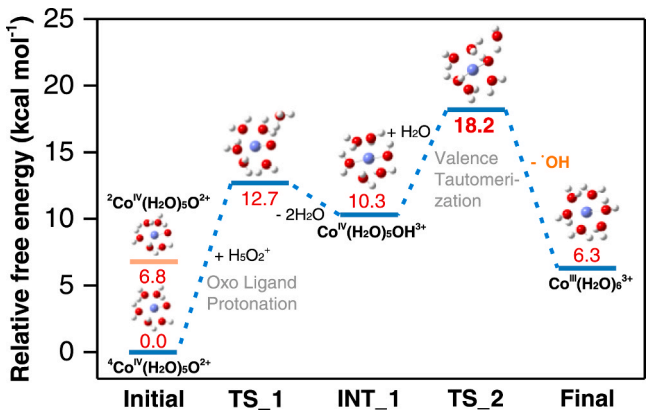

Fig. 4. Relative free energy surface for the proposed evolution pathway of •OH triggered by Co(IV) species at PBE0-D3BJ/TZVP/SMD(water) level.

and coordinated with an additional H_2O molecular to finally generate $Co^{III}(H_2O)_6$ (Eq. 10), with the energy barrier of 18.2 kcal mol^{-1}. The calculated pathway highlighted the significance of oxo ligand protonation-induced valence tautomerization in the evolution of •OH triggered by Co(IV) species. This result was consistent well with the literature reporting that high-valent metal-oxo species ($M^n=O^{2-}$) can transform into the corresponding metal-oxyl species ($M^{n-1}=O^{\bullet-}$) via the valence tautomerization, which is particularly likely for late transition metal-oxo complex (i.e., Co, Ni, Cu) due to the lower *d*-orbital energy induced inversion in M–O bonding [37,50], with the protonation of oxo-ligand promoting the following electron transfer between valence tautomers [51]. Besides, the calculated result also supported the above observations that the conversion of Co(IV) species to •OH deteriorated with the increase of pH, due to the indispensability of H^+ in the protonation of oxo ligand.

$$Co(IV)=O^{2+}+H^+\rightarrow Co(IV)-OH^{3+} \quad (9)$$

$$Co(IV)-OH^{3+}\rightarrow Co(III)+{}^{\bullet}OH \quad (10)$$

3.5. Substrate and concentration-dependent contribution of Co(IV) and •OH on the degradation of various organic contaminants

The respective contribution of Co(IV) and •OH on the oxidation of different organic contaminants were distinguished using TBA as the specific scavenger for •OH. As illustrated in Fig. 5a–g, excessive TBA exerted no inhibitory effect or merely slightly suppressed the degradation of sulfamethoxazole (SMX), sulfadiazine (SDZ), 2,4,6-trichlorophenol (TCP), acetaminophen (ACT), bisphenol A (BPA), diclofenac sodium (DCF) and carbamazepine (CBZ), demonstrating the negligible contribution of •OH on the oxidative removal of these parent contaminants. In contrast, TBA obviously inhibited the degradation of ibuprofen (IBU), nitrobenzene (NB) and 4-nitrobenzoic acid (4-NBA) (Fig. 5h–j). Especially for NB and 4-NBA that exclusively contain electron-withdrawn groups, TBA almost entirely restrained the oxidation of these two contaminants in the Co(II)/PMS process. UPLC-Q-TOF MS/MS tests likewise demonstrated that the degradation intermediates of NB and 4-NBA were mainly hydroxylated products (Figs. S24 and S25). Therefore, combined with the results from TBA scavenging experiments, it can be concluded

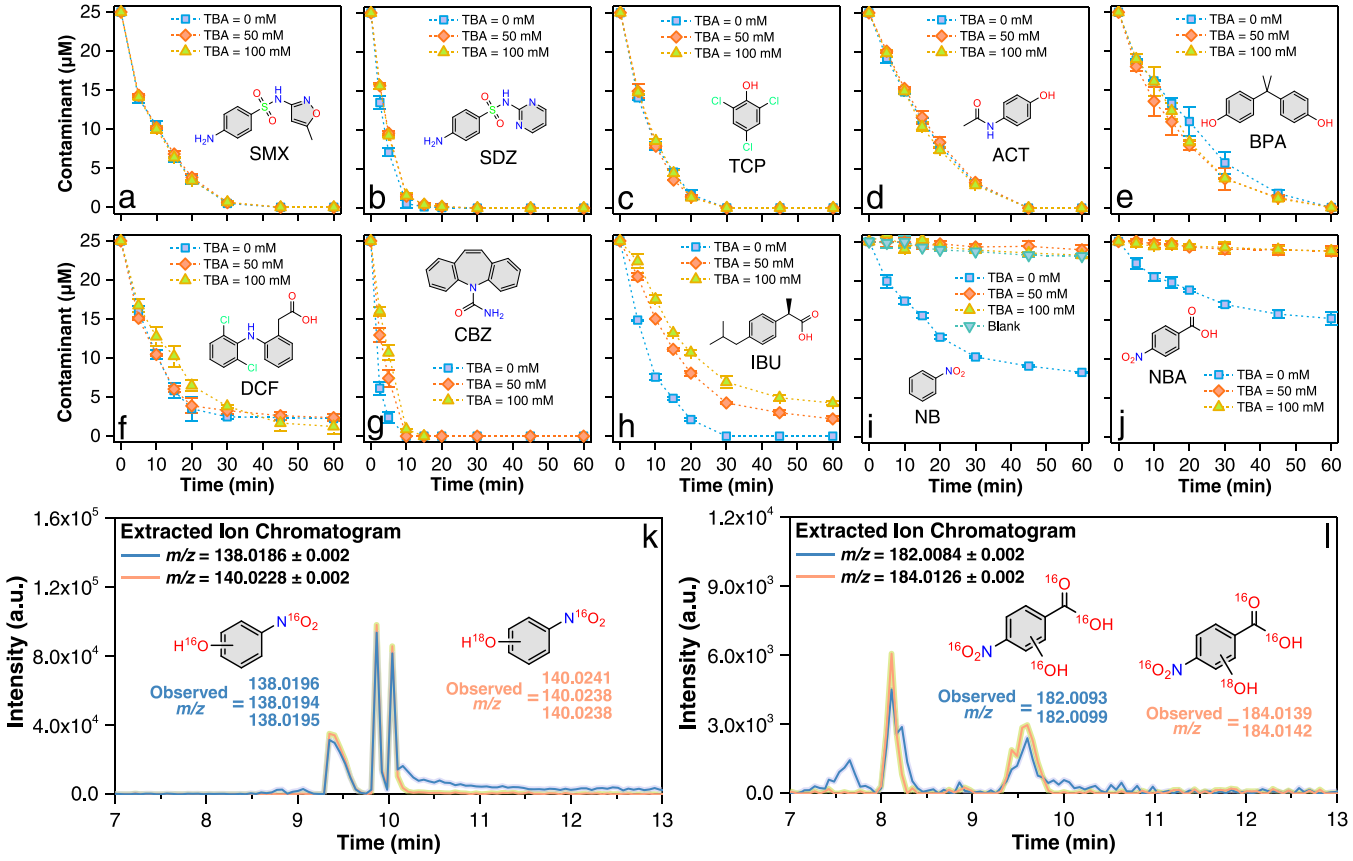

Fig. 5. Effect of TBA (0 –100 mM) on the degradation of SMX (a), SDZ (b), TCP (c), ACT (d), BPA (e), DCF (f), CBZ (g), IBU (h), NB (i), 4-NBA (j) in the Co(II)/PMS process, detection of NB–^{16}OH ($m/z = 138.0186 \pm 0.002$ [M – H]$^-$)/NB–^{18}OH ($m/z = 140.0228 \pm 0.002$ [M – H]$^-$) (k) and 4-NBA–^{16}OH ($m/z = 182.0084 \pm 0.002$ [M – H]$^-$)/ 4-NBA–^{18}OH ($m/z = 184.0126 \pm 0.002$ [M – H]$^-$) (l) during the oxidation of NB and 4-NBA in the Co(II)/PMS process in $H_2{}^{18}O$. Reaction conditions: pH = 3.0, $[Co(II)]_0 = 0.2$ mM, $[PMS]_0 = 0.2$ mM, $[SMX]_0 = [SDZ]_0 = [TCP]_0 = [ACT]_0 = [BPA]_0 = [DCF]_0 = [CBZ]_0 = [IBU]_0 = [NB]_0 = [4\text{-}NBA]_0 = 25$ μM for (a–j); pH = 3.0, $[Co(II)]_0 = 0.5$ mM, $[PMS]_0 = 2.5$ mM, $[NB]_0 = [4\text{-}NBA]_0 = 500$ μM for (k and l).

that •OH was dominantly responsible for the oxidation of NB and 4-NBA, instead of Co(IV) species.

The oxidation products of NB and 4-NBA in the Co(II)/PMS process in $H_2{}^{18}O$ were further investigated. As expected, ^{18}O-incorporated hydroxylated NB (noted as NB−^{18}OH, theoretical $m/z = 140.0228$ $[M - H]^-$) and ^{18}O-incorporated hydroxylated 4-NBA (noted as 4-NBA−^{18}OH, theoretical $m/z = 184.0126$ $[M - H]^-$) were generated (Fig. 5k, l, S26 and S27), with the proportion of NB−^{18}OH to NB−OH and 4-NBA−^{18}OH to 4-NBA−OH determined to be 48.5% and 56.6%, respectively. These values were consistent with those of $PMS^{16}O^{18}O$ to $PMSO_2$ (61.3%) and $PMS^{16}O^{16}O-^{18}OH$ to $PMSO_2$−OH (51.3%) as discussed above, which again indicated that •OH was triggered by Co(IV) species and thus the degradation of NB and 4-NBA were indirectly associated with Co(IV) under the tested conditions.

Nevertheless, despite that •OH was not the main reactive species responsible for the decay of most of tested contaminants, the potential contribution of •OH still needs to be carefully evaluated. For instance, in the case of ACT, TBA exerted no inhibitory effect on the decay of the parent contaminant, but remarkably suppressed the further degradation of an oxidized intermediate (Fig. S28). This was because in the initial stage of the reaction, Co(IV) preferred to react with ACT whose ionization potential value is relatively low [25,52], while with the decrease of ACT, the conversion of Co(IV) to •OH became prevailing, subsequently leading to the contribution of •OH being revealed. Such an oxidation characteristic highly resembled the above observations that the respective role of Co(IV) and •OH heavily relied on the relative concentration of PMSO. Therefore, these results interestingly and collectively demonstrated that the direct contribution of Co(IV) and •OH on organic oxidation was not only dependent on the type of the substrate, but also strongly related to its specific concentration, due to the different reactivity of Co(IV) and •OH and the unique transformation pathway of Co(IV) to •OH.

4. Conclusions

In this study, by systematically performing ^{18}O-isotope labeling assays, PMSO probe tests, DFT calculation and representative contaminants degradation experiments, the evolution pathway of •OH triggered by Co(IV) species via the protonation of oxo ligand-induced valence tautomerization was revealed for the first time. Despite that Co(IV) species only leads to •OH generation under acidic conditions, this is particularly significant for PMS-based AOPs since the employment of PMS inevitably acidifies the treated water matrix, which signifies the non-negligible role of Co(IV)-triggered •OH. More importantly, the binary cooperation of Co(IV) and •OH also endows the Co(II)/PMS process with selectivity and broad spectrum in contaminants abatement.

In addition, this study also highlights the remarkably varied oxidative contribution of non-radical species (i.e., Co(IV)) and radical species (i.e., •OH) on the degradation of different organic contaminants. For AOPs in which selective and non-selective species might intertwine together, it is no longer appropriate to investigate the respective role of various reactive species merely based on one model compound, instead a comprehensive evaluation is necessary. Besides, as a widely employed buffer species, the potential scavenging effect of acetic acid on radical species is also worthy of careful attention in future studies, which might have already led misinterpretations on experimental observations.

CRediT authorship contribution statement

Yang Zong: Conceptualization, Methodology, Investigation, Data curation, Writing – original draft, **Hua Zhang:** Investigation, Data curation, Writing – original draft, **Xiaomeng Zhang:** Resources, Investigation, Data curation, **Wen Liu:** Resources, Data curation, **Longqian Xu:** Resources, Data curation, **Deli Wu:** Validation, Supervision, Writing – review & editing, Funding acquisition.

Declaration of Competing Interest

The authors declare that they have no known competing financial interests or personal relationships that could have appeared to influence the work reported in this paper.

Acknowledgements

This work was financially supported by National Natural Science Foundation of China (Grants 21776223 and 52170091) and National Key R&D Program of China (2018YFC1903202). Yang Zong greatly appreciates the insightful discussions with Dr. Hongyu Dong from Tongji University before the preparation of this manuscript and the technical assistance from Dr. Binbin Shao and Tiansheng Chen of Tongji University.

Appendix A. Supporting information

Supplementary data associated with this article can be found in the online version at doi:10.1016/j.apcatb.2021.120722.

References

[1] G.P. Anipsitakis, D.D. Dionysiou, Degradation of organic contaminants in water with sulfate radicals generated by the conjunction of peroxymonosulfate with cobalt, Environ. Sci. Technol. 37 (2003) 4790–4797.
[2] G.P. Anipsitakis, D.D. Dionysiou, Radical generation by the interaction of transition metals with common oxidants, Environ. Sci. Technol. 38 (2004) 3705–3712.
[3] I.A. Ike, K.G. Linden, J.D. Orbell, M. Duke, Critical review of the science and sustainability of persulphate advanced oxidation processes, Chem. Eng. J. 338 (2018) 651–669.
[4] P. Hu, M. Long, Cobalt-catalyzed sulfate radical-based advanced oxidation: a review on heterogeneous catalysts and applications, Appl. Catal. B 181 (2016) 103–117.
[5] H. Dong, G. Wei, T. Cao, B. Shao, X. Guan, T.J. Strathmann, Insights into the oxidation of organic cocontaminants during Cr(VI) reduction by sulfite: the overlooked significance of Cr(V), Environ. Sci. Technol. 54 (2020) 1157–1166.
[6] Y. Gao, Y. Zhou, S.Y. Pang, J. Jiang, Z. Yang, Y. Shen, Z. Wang, P.X. Wang, L. H. Wang, New insights into the combination of permanganate and bisulfite as a novel advanced oxidation process: importance of high valent manganese-oxo species and sulfate radical, Environ. Sci. Technol. 53 (2019) 3689–3696.
[7] J. Zhu, F. Yu, J. Meng, B. Shao, H. Dong, W. Chu, T. Cao, G. Wei, H. Wang, X. Guan, Overlooked role of Fe(IV) and Fe(V) in organic contaminant oxidation by Fe(VI), Environ. Sci. Technol. 54 (2020) 9702–9710.
[8] J. Chen, D. Rao, H. Dong, B. Sun, B. Shao, G. Cao, X. Guan, The role of active manganese species and free radicals in permanganate/bisulfite process, J. Hazard. Mater. 388 (2020), 121735.
[9] Y. Zong, X. Guan, J. Xu, Y. Feng, Y. Mao, L. Xu, H. Chu, D. Wu, Unraveling the overlooked involvement of high-valent cobalt-oxo species generated from the cobalt(II)-activated peroxymonosulfate process, Environ. Sci. Technol. 54 (2020) 16231–16239.
[10] Z. Wang, J. Jiang, S. Pang, Y. Zhou, C. Guan, Y. Gao, J. Li, Y. Yang, W. Qiu, C. Jiang, Is sulfate radical really generated from peroxydisulfate activated by iron (II) for environmental decontamination? Environ. Sci. Technol. 52 (2018) 11276–11284.
[11] Z. Wang, W. Qiu, S. Pang, J. Jiang, Effect of chelators on the production and nature of the reactive intermediates formed in Fe(II) activated peroxydisulfate and hydrogen peroxide processes, Water Res. 164 (2019), 114957.
[12] Z. Wang, W. Qiu, S. Pang, Y. Gao, Y. Zhou, Y. Cao, J. Jiang, Relative contribution of ferryl ion species (Fe(IV)) and sulfate radical formed in nanoscale zero valent iron activated peroxydisulfate and peroxymonosulfate processes, Water Res. 172 (2020), 115504.
[13] O. Pestovsky, S. Stoian, E.L. Bominaar, X. Shan, E. Munck, L. Que Jr., A. Bakac, Aqueous FeIV==O: spectroscopic identification and oxo-group exchange, Angew. Chem. Int. Ed. 44 (2005) 6871–6874.
[14] M.S. Seo, J.-H. In, S.O. Kim, N.Y. Oh, J. Hong, J.K. Kim, L. Que Jr., W. Nam, Direct evidence for oxygen-atom exchange between nonheme oxoiron(IV) complexes and isotopically labeled water, Angew. Chem. Int. Ed. 43 (2004) 2417–2420.
[15] Y. Gao, H.P. Pan, Y. Zhou, Z. Wang, S.Y. Pang, C.T. Guan, Y.M. Shen, J. Jiang, Are free radicals actually responsible for enhanced oxidation of contaminants by Cr(VI) in the presence of bisulfite? Chemosphere 248 (2020), 126000.
[16] A. Ali, W. Akram, H.Y. Liu, Reactive cobalt(-)oxo complexes of tetrapyrrolic macrocycles and N-based ligand in oxidative transformation reactions, Molecules 24 (2019) 78–95.
[17] W. Nam, I. Kim, Y. Kim, C. Kim, Biomimetic alkane hydroxylation by cobalt(iii) porphyrin complex and m-chloroperbenzoic acid, Chem. Commun. (2001) 1262–1263.
[18] K. Ray, F. Heims, F.F. Pfaff, Terminal oxo and imido transition-metal complexes of groups 9-11, Eur. J. Inorg. Chem. 2013 (2013) 3784–3807.

[19] W.-Y. Zhou, P. Tian, F.-A. Sun, M.-Y. He, Q. Chen, Highly efficient transformation of alcohol to carbonyl compounds under a hybrid bifunctional catalyst originated from metalloporphyrins and hydrotalcite, J. Catal. 335 (2016) 105–116.
[20] W. Nam, M.H. Lim, S.K. Moon, C. Kim, Participation of two distinct hydroxylating intermediates in iron(III) porphyrin complex-catalyzed hydroxylation of alkanes, J. Am. Chem. Soc. 122 (2000) 10805–10809.
[21] C. Luo, M. Sadhasivan, J. Kim, V.K. Sharma, C.H. Huang, Revelation of Fe(V)/Fe (IV) involvement in the Fe(VI)-ABTS system: kinetic modeling and product analysis, Environ. Sci. Technol. 55 (2021) 3976–3987.
[22] V.K. Sharma, R. Zboril, R.S. Varma, Ferrates: greener oxidants with multimodal action in water treatment technologies, Acc. Chem. Res. 48 (2015) 182–191.
[23] J. Kim, T. Zhang, W. Liu, P. Du, J.T. Dobson, C.H. Huang, Advanced oxidation process with peracetic acid and Fe(II) for contaminant degradation, Environ. Sci. Technol. 53 (2019) 13312–13322.
[24] H. Dong, Y. Li, S. Wang, W. Liu, G. Zhou, Y. Xie, X. Guan, Both Fe(IV) and radicals are active oxidants in the Fe(II)/peroxydisulfate process, Environ. Sci. Technol. Lett. 7 (2020) 219–224.
[25] B. Liu, W. Guo, H. Wang, S. Zheng, Q. Si, Q. Zhao, H. Luo, N. Ren, Peroxymonosulfate activation by cobalt(II) for degradation of organic contaminants via high-valent cobalt-oxo and radical species, J. Hazard. Mater. 416 (2021), 125679.
[26] B. Liu, W. Guo, W. Jia, H. Wang, S. Zheng, Q. Si, Q. Zhao, H. Luo, J. Jiang, N. Ren, Insights into the oxidation of organic contaminants by Co(II) activated peracetic acid: the overlooked role of high-valent cobalt-oxo species, Water Res. 201 (2021), 117313.
[27] Z. Wang, J. Wang, B. Xiong, F. Bai, S. Wang, Y. Wan, L. Zhang, P. Xie, M. R. Wiesner, Application of cobalt/peracetic acid to degrade sulfamethoxazole at neutral condition: efficiency and mechanisms, Environ. Sci. Technol. 54 (2019) 464–475.
[28] J. Kim, P. Du, W. Liu, C. Luo, H. Zhao, C.H. Huang, Cobalt/peracetic acid: advanced oxidation of aromatic organic compounds by acetylperoxyl radicals, Environ. Sci. Technol. 54 (2020) 5268–5278.
[29] H. Li, Z. Zhao, J. Qian, B. Pan, Are free radicals the primary reactive species in Co (II)-mediated activation of proxymonosulfate? New evidence for the role of the Co (II)-peroxymonosulfate complex, Environ. Sci. Technol. 55 (2021) 6397–6406.
[30] M.J. Frisch, G.W. Trucks, H.B. Schlegel, G.E. Scuseria, M.A. Robb, J.R. Cheeseman, G. Scalmani, V. Barone, B. Mennucci, G.A. Petersson, Gaussian 09, Gaussian, Inc., Wallingford CT, 2009.
[31] S. Grimme, J. Antony, S. Ehrlich, H. Krieg, A consistent and accurate ab initio parametrization of density functional dispersion correction (DFT-D) for the 94 elements H-Pu, J. Chem. Phys. 132 (2010), 154104.
[32] A.V. Marenich, C.J. Cramer, D.G. Truhlar, Universal solvation model based on solute electron density and on a continuum model of the solvent defined by the bulk dielectric constant and atomic surface tensions, J. Phys. Chem. B 113 (2009) 6378–6396.
[33] P. Neta, V. Madhavan, H. Zemel, R.W. Fessenden, Rate constants and mechanism of reaction of sulfate radical anion with aromatic compounds, J. Am. Chem. Soc. 99 (1977) 163–164.
[34] G. Merga, C.T. Aravindakumar, B.S.M. Rao, H. Mohan, J.P. Mittal, Pulse radiolysis study of the reactionsof $SO_4^{\bullet-}$ with some substituted benzenes in aqueous solution, J. Chem. Soc. Faraday Trans. 90 (1994) 597–604.
[35] J. Van Buren, A.A. Cuthbertson, D. Ocasio, D.L. Sedlak, Ubiquitous production of organosulfates during treatment of organic contaminants with sulfate radicals, Environ. Sci. Technol. Lett. 8 (2021) 574–580.
[36] B. Shao, H. Dong, B. Sun, X. Guan, Role of ferrate(IV) and ferrate(V) in activating ferrate(VI) by calcium sulfite for enhanced oxidation of organic contaminants, Environ. Sci. Technol. 53 (2018) 894–902.
[37] V.A. Larson, B. Battistella, K. Ray, N. Lehnert, W. Nam, Iron and manganese oxo complexes, oxo wall and beyond, Nat. Rev. Chem. 4 (2020) 404–419.
[38] Y. Yang, X. Lu, J. Jiang, J. Ma, G. Liu, Y. Cao, W. Liu, J. Li, S. Pang, X. Kong, C. Luo, Degradation of sulfamethoxazole by UV, UV/H_2O_2 and UV/persulfate (PDS): formation of oxidation products and effect of bicarbonate, Water Res. 118 (2017) 196–207.
[39] S. Liang, L. Zhu, J. Hua, W. Duan, P.T. Yang, S.L. Wang, C. Wei, C. Liu, C. Feng, Fe^{2+}/HClO reaction produces $Fe^{IV}O^{2+}$: an enhanced advanced oxidation process, Environ. Sci. Technol. 54 (2020) 6406–6414.
[40] P. Zhang, S. Yuan, Production of hydroxyl radicals from abiotic oxidation of pyrite by oxygen under circumneutral conditions in the presence of low-molecular-weight organic acids, Geochim. Cosmochim. Acta 218 (2017) 153–166.
[41] Y. Zong, Y. Mao, L. Xu, D. Wu, Non-selective degradation of organic pollutants via dioxygen activation induced by Fe(II)-tetrapolyphosphate complexes: identification of reactive oxidant and kinetic modeling, Chem. Eng. J. 398 (2020), 125603.
[42] G.V. Buxton, C.L. Greenstock, W.P. Helman, A.B. Ross, Critical review of rate constants for reactions of hydrated electrons, hydrogen atoms and hydroxyl radicals (˙OH/˙O⁻) in Aqueous Solution, J. Phys. Chem. Ref. Data 17 (1988) 513–886.
[43] S.J. Hug, L. Olivier, Iron-catalyzed oxidation of arsenic(III) by oxygen and by hydrogen peroxide: pH-dependent formation of oxidants in the fenton reaction, Environ. Sci. Technol. 37 (2003) 2734–2742.
[44] F. Jacobsen, J. Holcman, K. Sehested, Reactions of the ferryl ion with some compounds found in cloud water, Int. J. Chem. Kinet. 30 (1998) 215–221.
[45] G. Bai, I. Spasojevi, B. Secerov, M. Mojovi, Spin-trapping of oxygen free radicals in chemical and biological systems: New traps, radicals and possibilities, Spectrochim. Acta Part A 69 (2008) 1354–1366.
[46] B. Wang, Y.M. Lee, W.Y. Tcho, S. Tussupbayev, S.T. Kim, Y. Kim, M.S. Seo, K. B. Cho, Y. Dede, B.C. Keegan, T. Ogura, S.H. Kim, T. Ohta, M.H. Baik, K. Ray, J. Shearer, W. Nam, Synthesis and reactivity of a mononuclear non-haem cobalt (IV)-oxo complex, Nat. Commun. 8 (2017) 14839.
[47] K.P. O'Halloran, C. Zhao, N.S. Ando, A.J. Schultz, T.F. Koetzle, P.M.B. Piccoli, B. Hedman, K.O. Hodgson, E. Bobyr, M.L. Kirk, S. Knottenbelt, E.C. Depperman, B. Stein, T.M. Anderson, R. Cao, Y.V. Geletii, K.I. Hardcastle, D.G. Musaev, W. A. Neiwert, X. Fang, K. Morokuma, S. Wu, P. Kogerler, C.L. Hill, Revisiting the polyoxometalate-based late-transition-metal-oxo complexes: the "Oxo Wall" stands, Inorg. Chem. 51 (2012) 7025–7031.
[48] Y. Zong, Y. Shao, Y. Zeng, B. Shao, L. Xu, Z. Zhao, W. Liu, D. Wu, Enhanced oxidation of organic contaminants by iron(II)-activated periodate: the significance of high-valent iron–oxo species, Environ. Sci. Technol. 55 (2021) 7634–7642.
[49] S.K. Ling, S. Wang, Y. Peng, Oxidative degradation of dyes in water using Co2+/H2O2 and Co2+/peroxymonosulfate, J. Hazard. Mater. 178 (2010) 385–389.
[50] G.K. Gransbury, B.N. Livesay, J.T. Janetzki, M.A. Hay, R.W. Gable, M.P. Shores, A. Starikova, C. Boskovic, Understanding the origin of one- or two-step valence tautomeric transitions in bis(dioxolene)-bridged dinuclear cobalt complexes, J. Am. Chem. Soc. 142 (2020) 10692–10704.
[51] C.J. Bougher, S. Liu, S.D. Hicks, M.M. Abu-Omar, Valence tautomerization of high-valent manganese(V)-oxo corrole induced by protonation of the oxo ligand, J. Am. Chem. Soc. 137 (2015) 14481–14487.
[52] P. Hu, H. Su, Z. Chen, C. Yu, Q. Li, B. Zhou, P.J.J. Alvarez, M. Long, Selective degradation of organic pollutants using an efficient metal-free catalyst derived from carbonized polypyrrole via peroxymonosulfate activation, Environ. Sci. Technol. 51 (2017) 11288–11296.